Composites Communications 15 (2019) 162–167

Contents lists available at ScienceDirect

Composites Communications

journal homepage: www.elsevier.com/locate/coco

Short Communication

Confined sulfidation strategy toward cobalt sulfide@nitrogen, sulfur co-doped carbon core-shell nanocomposites for lithium-ion battery anodes

Le Li[a], Jun Zhou[a], Chao Zhang[a,*], Tianxi Liu[a,b,**]

[a] State Key Laboratory for Modification of Chemical Fibers and Polymer Materials, College of Materials Science and Engineering, Innovation Center for Textile Science and Technology, Donghua University, Shanghai, 201620, PR China

[b] Key Laboratory of Synthetic and Biological Colloids, Ministry of Education, School of Chemical and Material Engineering, Jiangnan University, Wuxi, 214122, PR China

ARTICLE INFO

Keywords:
Confined sulfidation
Core-shell nanocomposites
Nitrogen and sulfur dual-doping
Lithium-ion battery anodes

ABSTRACT

A confined sulfidation strategy is developed for the preparation of cobalt sulfide@nitrogen, sulfur co-doped carbon composites (CoS@NSC) with a unique core-shell structure. The as-fabricated CoS@NSC composites are beneficial for efficient lithium ion diffusion, fast electron transfer and improved structural integrity. As a demonstration, the CoS@NSC, as an anode material for lithium-ion battery, exhibits a high initial stable discharge capacity of 754 mA h g^{-1} and high capacity retention by maintaining 635 mA h g^{-1} at 1 A g^{-1} after 100 charge/discharge cycles. This confined sulfidation strategy can be readily extended to a large-scale and cost-effective production of other transition metal sulfide@carbon core-shell nanocomposites.

1. Introduction

The ever-growing demands for high-efficiency energy storage devices have been aroused in recent years [1–4]. Lithium ion battery (LIB) is one of the promising high-efficiency energy storage devices for electrical vehicles, portable electronic devices and back-up electricity storage units [5]. Researches on the battery technology focus on the development of electrode materials with high capacity, long cycle life and good rate capability [6,7]. Graphite, a commercial anode material for LIB, hinders the development of high-energy-density LIB due to its relatively low specific capacity. Great efforts have been made to develop novel anode materials for high-performance LIB including the transition metal sulfides (TMSs) [8,9]. TMSs typically exhibit high theoretical specific capacitances for LIB anodes, based on reversible redox reactions through the conversion reaction mechanism [10,11]. TMS electrodes can deliver about two or three times higher capacities than that of commercial graphite anodes [12–14]. However, TMS electrodes still meet some drawbacks inducing unsatisfied performance for their LIB applications [15–17]. The intrinsic low electrical and ion conductivity of TMSs inevitably induce inferior rate performance during cycling the lithium [18,19]. Besides, the pulverization of the unstable TMS electrode structure, caused by large volume changes during the repeated lithium uptake and removal processes, will cause their rapid capacity fading and poor cycle stability [20–22].

To address these issues mentioned above, many efforts have been focused to improve electrochemical performance of TMS electrodes by tailoring their compositions and structures [1,23–25]. The employment of conductive carbon components as an effective support to fabricate TMS-based composites is an effective strategy to alleviate the volume changes induced by lithium insertion/extraction and improve the electrical conductivity of electrode matrix [26,27]. However, simple compositions of TMSs with carbon materials are not able to deliver excellent electrochemical performance since a large proportion of exposed TMSs are not well protected from side reaction and volume changes [28]. Besides, the development of TMSs with tailored nanostructures, such as nanosheet, nanotube, york-shell and core-shell nanostructure, is another effective strategy to improve their electrochemical performance due to increased surface areas and decreased ion diffusion length [29–34]. Therefore, it is of great significance to fabricate TMS/carbon composites with precisely controlled nanostructures to further optimize their electrochemical performance.

Herein, a confined sulfidation strategy using sulfur powder as the sulfur source is presented for the preparation of cobalt sulfide@nitrogen, sulfur co-doped carbon composites (CoS@NSC) with a unique core-shell structure. Co-Al layered double hydroxide (Co-Al LDH) hexagon nanosheets with uniform polydopamine (PDA) coating were used as the precursor. During the confined sulfidation process, the Co-Al LDH core converted into porous CoS nanosheets, while the PDA shell

* Corresponding author.
** Corresponding author. State Key Laboratory for Modification of Chemical Fibers and Polymer Materials, College of Materials Science and Engineering, Innovation Center for Textile Science and Technology, Donghua University, Shanghai, 201620, PR China.
E-mail addresses: czhang@dhu.edu.cn (C. Zhang), txliu@fudan.edu.cn (T. Liu).

https://doi.org/10.1016/j.coco.2019.07.010
Received 17 June 2019; Received in revised form 25 July 2019; Accepted 25 July 2019
Available online 29 July 2019

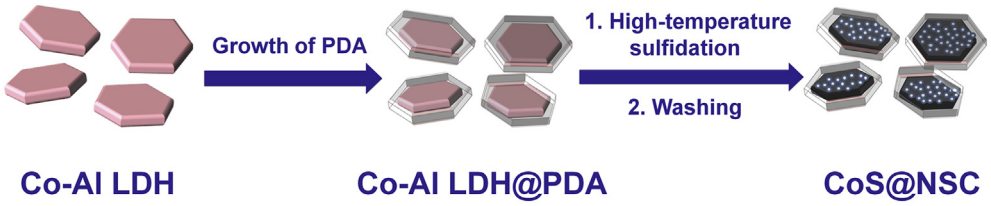

Fig. 1. Schematic of the preparation procedure of CoS@NSC composites.

was pyrolyzed into NSC layers at the high temperature. When used as anode materials for LIB, the CoS@NSC electrode exhibited remarkable electrochemical performance with a high reversible capacity, good rate capability and cycling stability.

2. Results and discussion

Fig. 1 illustrates the preparation procedure of the CoS@NSC composites. First, Co-Al LDH nanosheets were synthesized by a co-deposition method. Second, the Co-Al LDH nanosheets were used as a 2D template for an in-situ growth of a polydopamine (PDA) shell, thus to obtain a core-shelled Co-Al LDH@PDA composite. Third, the Co-Al LDH@PDA composites were converted into the CoS@NSC composites by high-temperature sulfidation using sublimed sulfur as the sulfur source. During the high-temperature sulfidation, the Co-Al LDH core was sulfided into porous CoS nanosheets, while the PDA shell was converted into nitrogen and sulfur co-doped carbon at high sulfidation temperature. The CoS@NSC-1, CoS@NSC-2 and CoS@NSC-3 represent the products prepared at the sulfidation temperature of 400, 600 and 800 °C, respectively. Control sample of CoS was prepared by using neat Co-Al LDH as the precursor at the sulfidation temperature of 600 °C.

The morphologies of as-prepared Co-Al LDH and Co-Al LDH@PDA were characterized by SEM observations. Neat Co-Al LDH exhibits a hexagon morphology with uniform sizes (Fig. 2a–b). The rough surface of the Co-Al LDH@PDA clearly indicates the successful coating of the PDA shell on the Co-Al LDH template (Fig. 2c–d). X-ray diffraction (XRD) analysis was employed to gain insight into crystalline structures of the Co-Al LDH, Co-Al LDH@PDA, CoS and CoS@NSC (Figs. S1 and 2e). The characteristic diffraction patterns of Co-Al LDH correspond to (003), (006), (012), (015) and (018) crystalline planes, respectively (Fig. S1a), confirming the synthesis of Co-Al LDH through the co-deposition method derived from mixed solution of cobalt salt, aluminum salt and urea [35,36]. Upon the coating with PDA shells, sharp characteristic diffraction patterns of (003) and (006) crystalline planes maintain well for the Co-Al LDH@PDA, indicating that there is no evident crystalline structure change in the process of PDA coating on the Co-Al LDH (Fig. S1b). Fig. 2e demonstrates that the diffraction patterns of the CoS@NSC and CoS correspond with spinel CoS (JCPDF No. 65-3418). In details, a series of sharp and well-defined diffraction patterns at $2\theta = 30.6^{\circ}$, 35.2°, 46.9° and 54.4° corresponds to (100), (101), (102) and (110) crystalline planes, respectively, suggesting that the as-synthesized CoS@NSC has a good crystallinity of spinel CoS. Raman spectra plays an important role in detecting chemical structures of carbon materials. Raman spectra of the CoS@NSC-1, CoS@NSC-2 and CoS@NSC-3 include two typical peaks at ~1350 and 1560 cm^{-1}, which correspond to D band (amorphous carbon) and G band (graphitic carbon) (Fig. 2f), respectively. For comparison, no noticeable Raman peaks ascribing to carbon structures are observed in the CoS. Raman spectra also indicates the graphitization degrees of pyrolyzed carbon shells derived from the PDA. The intensity ratio of the D and G bands (I_D/I_G) follows the order of CoS@NSC-3 (0.75) < CoS@NSC-1 (0.88) < CoS@NSC-2 (0.93). The higher I_D/I_G ratio indicates more disordered carbon structures within the CoS@NSC composites due to the efficient nitrogen and sulfur doping [37].

SEM images of as-prepared CoS@NSC were shown in Fig. 3a–f, which almost preserve the uniform hexagon nanosheet morphology of the Co-Al LDH@PDA. However, more fragments instead of uniform hexagon nanosheets are observed for the CoS without PDA coating (Fig. S2), which indicates a unique protective role of PDA coating for maintaining 2D nanosheet morphology. Besides, tiny carbon particles are also observed on the surface of CoS@NSC, which is due to the carbonization of excess PDA coating. The hexagon structure is well maintained for the CoS@NSC-1 and CoS@NSC-2, while a large proportion of fragments are observed for the CoS@NSC-3. The interior structure of the CoS@NSC-2 is further investigated by TEM (Fig. 3g–i). Fig. 3g presents the representative core-shell nanosheet structure of the

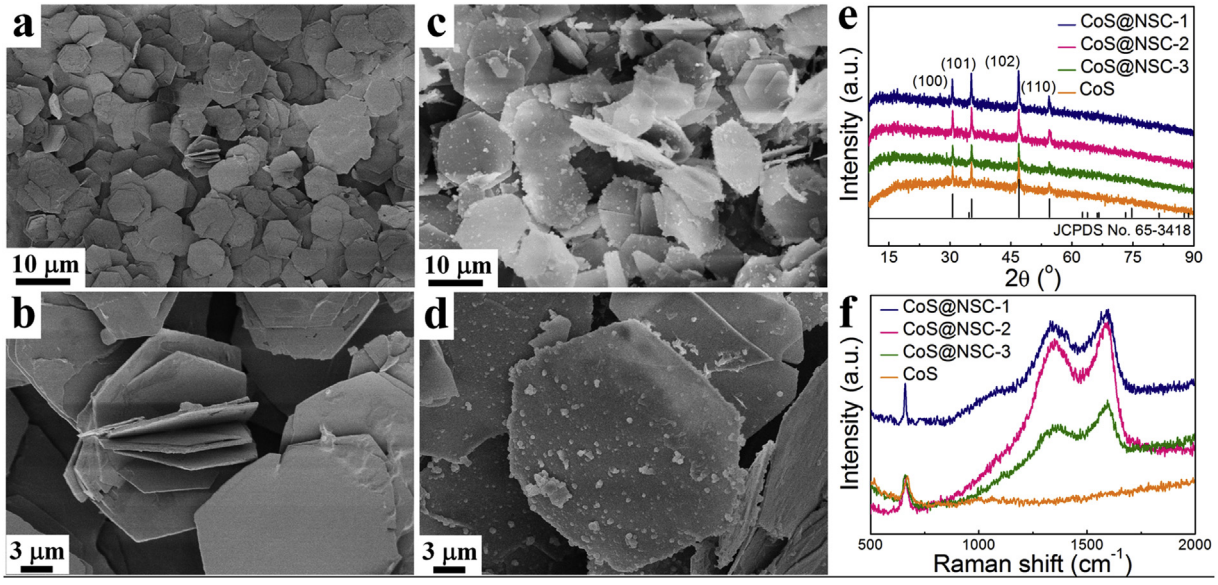

Fig. 2. SEM images of (a, b) Co-Al LDH and (c, d) Co-Al LDH@PDA. (e) XRD patterns and (f) Raman spectra of CoS, CoS@NSC-1, CoS@NSC-2 and CoS@NSC-3.

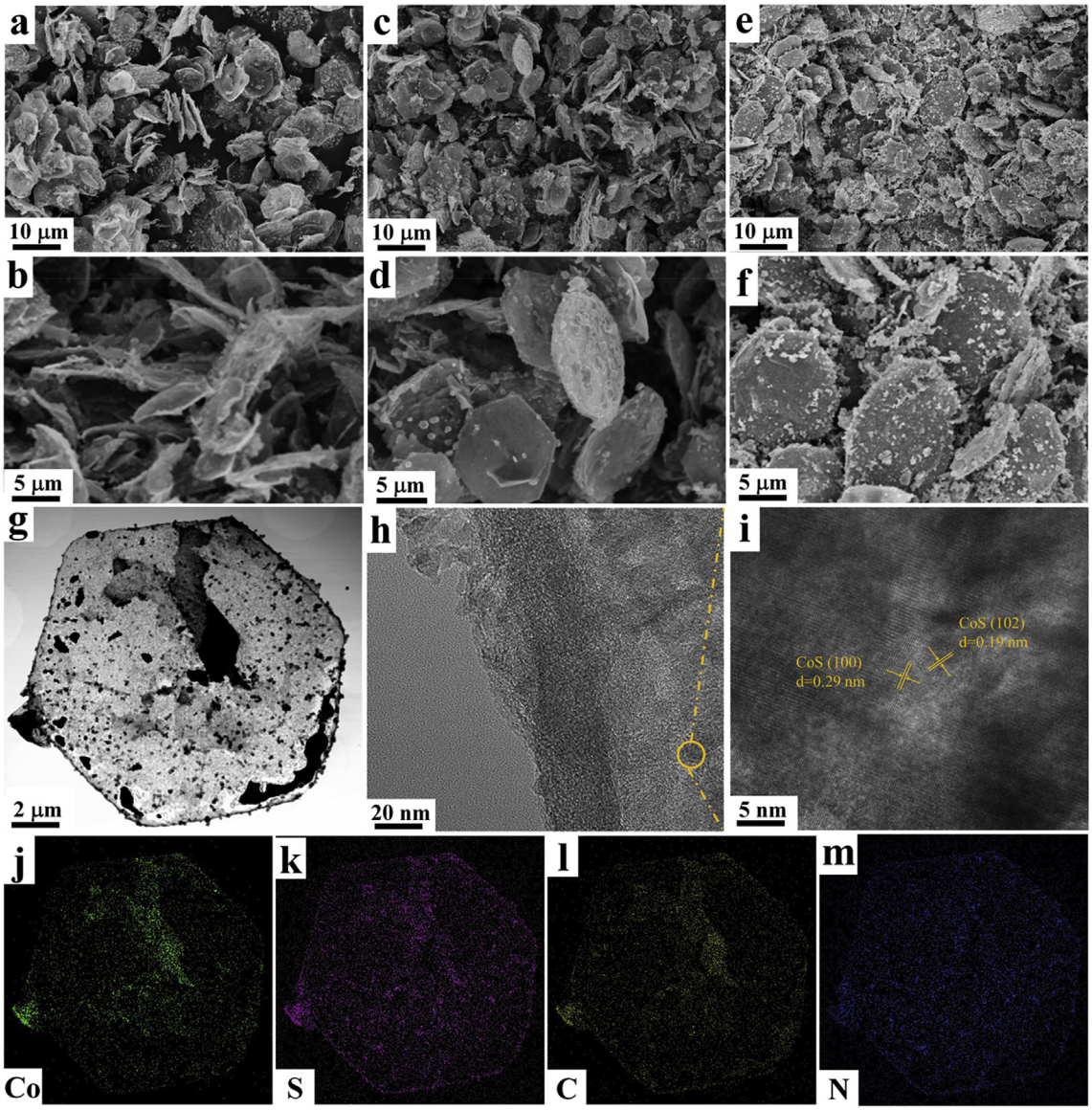

Fig. 3. SEM images of (a, b) CoS@NSC-1, (c, d) CoS@NSC-2 and (e, f) CoS@NSC-3. (g, h) TEM and (i) HRTEM images of CoS@NSC-2. Elements mappings of CoS@NSC-2 of (j) Co, (k) S, (l) C and (m) N elements.

CoS@NSC-2 with an obvious carbon shell on hexagon nanosheet core. The thickness of continuous carbon shell within the CoS@NSC-2 is calculated about 20 nm from high-magnification TEM image (Fig. 3h). The CoS cores within CoS@NSC-2 showing lattice fringes with the spacing of 0.29 and 0.19 nm (Fig. 3i), correspond to (100) and (102) planes of spinel CoS, which is in good agreement with XRD results. Elemental mappings reveal that the CoS@NSC-2 is a well-designed core-shell structure with uniformly distributed Co, S, C and N elements (Fig. 3j–m). The contents of N and S element in CoS@NSC-2 composites are calculated to be 13.4 wt% and 8.1 wt%, respectively, from elemental mapping results. The sufficient N and S doping in the NSC shell originate from N-rich components of PDA and subsequent sulfidation process, respectively.

Half coin cells with lithium foil as the counter electrode were assembled to evaluate the lithium storage ability of the CoS@NSC. The electrochemical measurements were performed in the potential window of 0.01-3.0 V. Fig. 4a shows the cyclic voltammetry (CV) curves of the CoS@NSC-2 electrode at a scan rate of 0.1 mV s^{-1} to determine its reversible redox process. The 1st cathodic scan of the CoS@NSC-2 demonstrates a sharp peak at ~1.25 V corresponding to the reduction of Co^{2+} to metallic Co, and a small peak at ~1.58 V relates to an irreversible reaction to form the solid electrolyte interphase (SEI). The sharp oxidation peak at ~2.03 V is attributed to the oxidation of metallic Co into CoS. After the 1st cycle, CV curves of the 2nd and 5th cycles are overlapped with similar redox peaks, indicating a reversible electrochemical process of electrochemical reaction in the core-shell CoS@NSC-2 electrode. The electrochemical cycling performance of the CoS@NSC-2 electrode is further evaluated by galvanostatic charging/discharging (GCD) at a current density of 1 A g^{-1} in the potential range of 0.01-3.0 V vs. Li/Li^+. Fig. 4b indicates one pair of well defined plateaus for the CoS@NSC-2, which is in good agreement with the CV results. During the 1st cycle, the high discharge/charge capacities of 1099 and 728 mA h g^{-1} are obtained. At the 5th cycle, the discharge capacity decreases to 754 mA h g^{-1}. The electrochemical performance for CoS@NSC-2 electrode is much better than that of the CoS@NSC-1 and CoS@NSC-3 electrodes (Fig. S3) with largely improved specific capacity and capacity retention in the following GCD cycles. Fig. 4c shows the rate capabilities of the CoS@NSC and CoS electrodes at various current densities. All the CoS@NSC electrodes exhibit higher specific capacity and stability than that of the CoS electrode especially

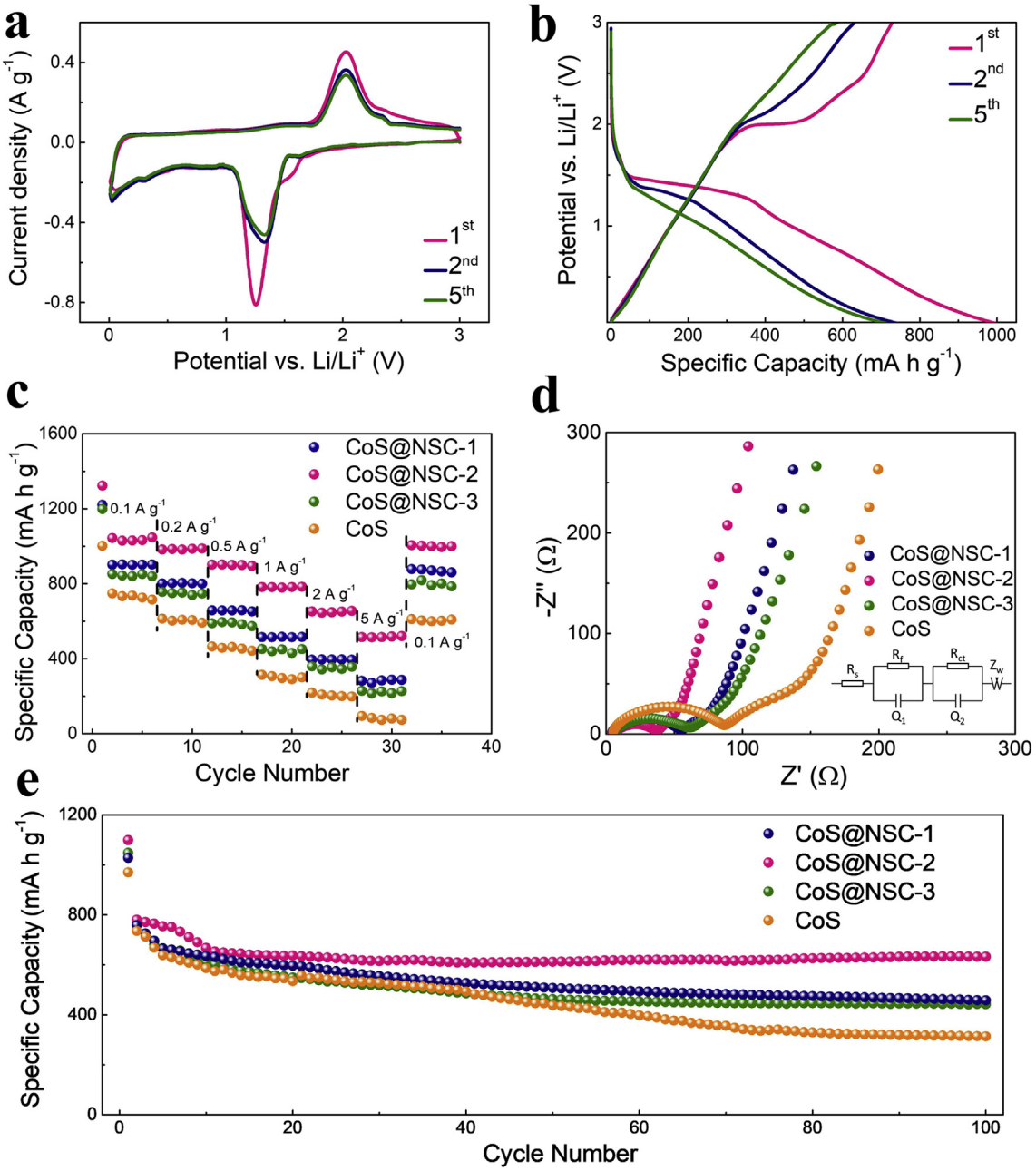

Fig. 4. (a) CV curves of CoS@NSC-2 electrode for 1st, 2nd and 5th cycle at 0.1 mV s^{-1} within the potential range of 0.01-3.0 V. (b) GCD profiles of CoS@NSC-2 electrode for 1st, 2nd and 5th cycle at 1 A g^{-1}. (c) Rate capacity of CoS, CoS@NSC-1, CoS@NSC-2 and CoS@NSC-3 electrodes. (d) EIS curves of CoS, CoS@NSC-1, CoS@NSC-2 and CoS@NSC-3 electrodes. Inset of (d) is corresponding equivalent circuit model. (e) Cycling performance of CoS, CoS@NSC-1, CoS@NSC-2 and CoS@NSC-3 electrodes at 1 A g^{-1}.

at high current density. The CoS@NSC-2 electrode delivers the highest capacity at various current densities among all the CoS@NSC electrodes, which is attributed to the unique confinement of the NSC shell around the CoS core. The electrochemical impedance spectroscopy (EIS) represented in terms of Nyquist plots consists of high-frequency and low-frequency regions (Fig. 4d), respectively. Inset of Fig. 4d shows the fitted equivalent circuits according to the measured EIS curves. In the equivalent circuits, the R_s, R_f and R_{ct} represent the current collector/electrolyte resistance, SEI layer resistance and charge-transfer resistance, respectively, and the Q_1, Q_2 and Z_w represent the constant phase element (CPE), double layer capacitance, Warburg impedance, respectively. The R_{ct} of CoS@NSC-2 electrode (35.2 Ω) is the smallest among CoS@NSC composites and CoS electrodes. Fig. 4e shows the cycling stability of the CoS@NSC and CoS electrodes at a current density of 1 A g^{-1} in the potential range from 0.01 to 3.0 V vs. Li/Li^+. The CoS@NSC-2 electrode delivers a reversible specific capacity of 635 mA h g^{-1} without obvious capacity decay after 100 cycles, which further demonstrates its good reversibility of the lithiation/delithiation process. For comparison, neat CoS electrode without the NSC shell typically shows a rapid capacity decay after 100 cycles, reaching a discharge capacity of 310 mA h g^{-1}. These results further demonstrate the superior cycling stability of the CoS@NSC-2 electrode due to the protective effect of NSC shells.

The excellent lithium storage performance of the CoS@NSC-2 electrode, in terms of large specific capacity, superior cycle stability and excellent rate capability, is attributed to the unique structural features of porous CoS nanosheets and surrounded NSC shells. First, 2D porous CoS nanosheets allow an enhanced kinetic rate for lithium ions with

short insertion/extraction diffusions, which is critical for lithium ion diffusion especially during fast discharge and charge process. The porous CoS structure also offers a sufficient void space to effectively accommodate volume changes induced by insertion/extraction of lithium ions and thus alleviate mechanical stress caused by volume change, resulting in stable electrode structures with excellent cycling performance. Second, the presence of surrounded N, S co-doped NSC shells also enhances the charge transportation throughout core-shell structure with the obvious smaller charge transfer resistance [26,38,39]. The NSC shell also functions as a buffering layer to relieve the volume expansion of embedded CoS nanosheets and thus improve the structural integrity.

3. Conclusion

In summary, the Co-Al LDH nanosheets were used as a 2D template for a uniform growth of PDA, thus to obtain the Co-Al LDH@PDA composites. The CoS@NSC composites with a unique core-shell structure were prepared by confined sulfidation strategy, using the Co-Al LDH@PDA and sulfur powder as the precursor and sulfur source, respectively. The NSC shells on CoS cores can greatly enhance the electrical conductivity and accommodate the volume expansion during the charge/discharge process. When employed as anode materials for LIB, the CoS@NSC electrodes can achieve highly efficient and stable lithium ion storage with an ultrahigh initial capacity of 635 mA h g^{-1} and a long lifespan of 100 cycles at the current density of 1 A g^{-1}. The largely enhanced electrochemical performance of the CoS@NSC composites is attributed to the unique 2D hexagon nanosheet morphology of porous CoS confined in an NSC shell, which can efficiently reduce the ion diffusion length, buffer the volume expansion during ion insertion/extraction process. This study may provide a simple and efficient way for the design and preparation of novel metal sulfide-based composites for the applications in high-performance LIB.

Acknowledgements

We are grateful for the financial support from the National Natural Science Foundation of China (51773035, 51433001), the Natural Science Foundation of Shanghai (17ZR1439900), the Program of Shanghai Subject Chief Scientist (17XD1400100), and the Shanghai Scientific and Technological Innovation Project (18JC1410600).

Appendix A. Supplementary data

Supplementary data to this article can be found online at https://doi.org/10.1016/j.coco.2019.07.010.

References

[1] Z. Hu, Q. Liu, S.L. Chou, S.X. Dou, Advances and challenges in metal sulfides/selenides for next-generation rechargeable sodium-ion batteries, Adv. Mater. 29 (2017) 1700606.
[2] L. Li, K. Wang, Z. Huang, C. Zhang, T.X. Liu, Highly ordered graphene architectures by duplicating melamine sponges as a three-dimensional deformation-tolerant electrode, Nano Res. 9 (2016) 2938–2949.
[3] Z. Huang, L. Li, Y. Wang, C. Zhang, T.X. Liu, Polyaniline/graphene nanocomposites towards high-performance supercapacitors: a review, Compos. Commun. 8 (2018) 83–91.
[4] Y.T. Zhou, J. Yang, H.Q. Liang, J.K. Pi, C. Zhang, Z.K. Xu, Sandwich-structured composite separators with an anisotropic pore architecture for highly safe Li-ion batteries, Compos. Commun. 8 (2018) 46–51.
[5] T. Zhang, T. Tian, B. Shen, Y. Song, H. Yao, Recent advances on biopolymer fiber based membranes for lithium-ion battery separators, Compos. Commun. 14 (2019) 7–14.
[6] J. Zhou, Y. Wang, C. Zhang, Synthesis and electrochemical performance of core-shell NiCo2S4@nitrogen, sulfur dual-doped carbon composites via confined sulfidation strategy in a polydopamine nanoreactor, Compos. Commun. 12 (2019) 74–79.
[7] S. Li, Z. Cui, D. Li, G. Yue, J. Liu, H. Ding, et al., Hierarchically structured electrospinning nanofibers for catalysis and energy storage, Compos. Commun. 13 (2019) 1–11.
[8] C. Wu, Y. Jiang, P. Kopold, P.A. van Aken, J. Maier, Y. Yu, Peapod-like carbon-encapsulated cobalt chalcogenide nanowires as cycle-stable and high-rate materials for sodium-ion anodes, Adv. Mater. 28 (2016) 7276–7283.
[9] Y. Xu, T. Yuan, Z. Bian, H. Sun, Y. Pang, C. Peng, et al., Electrospun flexible Si/C@CNF nonwoven anode for high capacity and durable lithium-ion battery, Compos. Commun. 11 (2019) 1–5.
[10] Y. Lin, Z. Qiu, D. Li, S. Ullah, Y. Hai, H. Xin, et al., NiS2@CoS2 nanocrystals encapsulated in N-doped carbon nanocubes for high performance lithium/sodium ion batteries, Energy Storage Mater. 11 (2018) 67–74.
[11] Y. Shim, R.M. Young, A.P. Douvalis, S.M. Dyar, B.D. Yuhas, T. Bakas, et al., Enhanced photochemical hydrogen evolution from Fe4S4-based biomimetic chalcogels containing M2+ (M = Pt, Zn, Co, Ni, Sn) centers, J. Am. Chem. Soc. 136 (2014) 13371–13380.
[12] C. Tan, H. Zhang, Two-dimensional transition metal dichalcogenide nanosheet-based composites, Chem. Soc. Rev. 44 (2015) 2713–2731.
[13] X. Yin, C. Tang, M. Chen, S. Adams, H. Wang, H. Gong, Hierarchical porous Cu2ZnSnS4 films for high-capacity reversible lithium storage applications, J. Mater. Chem. A 1 (2013) 7927–7932.
[14] Q. Zhang, Z. Xu, B. Lu, Strongly coupled MoS2–3D graphene materials for ultrafast charge slow discharge LIBs and water splitting applications, Energy Storage Mater. 4 (2016) 84–91.
[15] Y. Liu, Y. Li, H. Kang, T. Jin, L. Jiao, Design, synthesis, and energy-related applications of metal sulfides, Mater. Horiz. 3 (2016) 402–421.
[16] Y. Zhou, D. Yan, H. Xu, J. Feng, X. Jiang, J. Yue, et al., Hollow nanospheres of mesoporous Co9S8 as a high-capacity and long-life anode for advanced lithium ion batteries, Nano Energy 12 (2015) 528–537.
[17] X. Song, X. Li, Z. Bai, B. Yan, D. Li, X. Sun, Morphology-dependent performance of nanostructured Ni3S2/Ni anode electrodes for high performance sodium ion batteries, Nano Energy 26 (2016) 533–540.
[18] S.H. Choi, Y.C. Kang, Synthesis for yolk-shell-structured metal sulfide powders with excellent electrochemical performances for lithium-ion batteries, Small 10 (2014) 474–478.
[19] X.-Y. Yu, H. Hu, Y. Wang, H. Chen, X.W. Lou, Ultrathin MoS2 nanosheets supported on N-doped carbon nanoboxes with enhanced lithium storage and electrocatalytic properties, Small 54 (2015) 7395–7398.
[20] F. Jin, Y. Wang, Topotactical conversion of carbon coated Fe-based electrodes on graphene aerogels for lithium ion storage, J. Mater. Chem. A 3 (2015) 14741–14749.
[21] H. Yu, H. Fan, X. Wu, H. Wang, Z. Luo, H. Tan, et al., Diffusion induced concave Co3O4@CoFe2O4 hollow heterostructures for high performance lithium ion battery anode, Energy Storage Mater. 4 (2016) 145–153.
[22] S. Xiao, X. Li, W. Sun, B. Guan, Y. Wang, General and facile synthesis of metal sulfide nanostructures: in situ microwave synthesis and application as binder-free cathode for Li-ion batteries, Chem. Eng. J. 306 (2016) 251–259.
[23] Y. Zhao, L.P. Wang, M.T. Sougrati, Z. Feng, Y. Leconte, A. Fisher, et al., A review on design strategies for carbon based metal oxides and sulfides nanocomposites for high performance Li and Na ion battery anodes, Adv. Energy Mater. 7 (2017) 1601424.
[24] L. Chen, Y. Zhang, C. Lin, W. Yang, Y. Meng, Y. Guo, et al., Hierarchically porous nitrogen-rich carbon derived from wheat straw as an ultra-high-rate anode for lithium ion batteries, J. Mater. Chem. A 2 (2014) 9684–9690.
[25] Y. Zhao, X. Li, B. Yan, D. Xiong, D. Li, S. Lawes, et al., Recent developments and understanding of novel mixed transition-metal oxides as anodes in lithium ion batteries, Adv. Energy Mater. 6 (2016) 1502175.
[26] Y. Chen, X. Li, K. Park, J. Song, J. Hong, L. Zhou, et al., Hollow carbon-nanotube/carbon-nanofiber hybrid anodes for Li-ion batteries, J. Am. Chem. Soc. 135 (2013) 16280–16283.
[27] P. Geng, S. Zheng, H. Tang, R. Zhu, L. Zhang, S. Cao, et al., Transition metal sulfides based on graphene for electrochemical energy storage, Adv. Energy Mater. 8 (2018) 1703259.
[28] X. Xu, W. Liu, Y. Kim, J. Cho, Nanostructured transition metal sulfides for lithium ion batteries: progress and challenges, Nano Today 9 (2014) 604–630.
[29] B. Chen, N. Zhao, L. Guo, F. He, C. Shi, C. He, et al., Facile synthesis of 3D few-layered MoS2 coated TiO2 nanosheet core–shell nanostructures for stable and high-performance lithium-ion batteries, Nanoscale 7 (2015) 12895–12905.
[30] Q. Wang, R. Zou, W. Xia, J. Ma, B. Qiu, A. Mahmood, et al., Facile synthesis of ultrasmall CoS2 nanoparticles within thin N-doped porous carbon shell for high performance lithium-ion batteries, Small 11 (2015) 2511–2517.
[31] R. Wu, D.P. Wang, X. Rui, B. Liu, K. Zhou, A.W.K. Law, et al., In-situ formation of hollow hybrids composed of cobalt sulfides embedded within porous carbon polyhedra/carbon nanotubes for high-performance lithium-ion batteries, Adv. Mater. 27 (2015) 3038–3044.
[32] X.-Y. Yu, L. Yu, X.W. Lou, Metal sulfide hollow nanostructures for electrochemical energy storage, Adv. Energy Mater. 6 (2016) 1501333.
[33] H. Guo, Q. Feng, K. Xu, J. Xu, J. Zhu, C. Zhang, et al., Self-templated conversion of metallogel into heterostructured TMP@carbon quasiaerogels boosting bifunctional electrocatalysis, Adv. Funct. Mater. (2019), https://doi.org/10.1002/adfm.201903660.
[34] H. Lu, Y. Zhang, Y. Huang, C. Zhang, T. Liu, Reaction packaging CoSe2 nanoparticles in N-doped carbon polyhedra with bifunctionality for overall water splitting, ACS Appl. Mater. Interfaces 11 (2019) 3372–3381.
[35] J. Xu, S. Gai, F. He, N. Niu, P. Gao, Y. Chen, et al., Reduced graphene oxide/Ni(1-x)Co(x)Al-layered double hydroxide composites: preparation and high supercapacitor performance, Dalton Trans. 43 (2014) 11667–11675.
[36] L.-H. Su, X.-G. Zhang, Y. Liu, Electrochemical performance of Co–Al layered double hydroxide nanosheets mixed with multiwall carbon nanotubes, J. Solid State

Electrochem. 12 (2007) 1129–1134.
[37] W. Ai, Z. Luo, J. Jiang, J. Zhu, Z. Du, Z. Fan, et al., Nitrogen and sulfur codoped graphene: multifunctional electrode materials for high-performance Li-ion batteries and oxygen reduction reaction, Adv. Mater. 26 (2014) 6186–6192.
[38] H. Guo, Q. Feng, J. Zhu, J. Xu, Q. Li, S. Liu, et al., Cobalt nanoparticle-embedded nitrogen-doped carbon/carbon nanotube frameworks derived from a metal–organic framework for tri-functional ORR, OER and HER electrocatalysis, J. Mater. Chem. A 7 (2019) 3664–3672.
[39] S. Chen, Y. Zheng, B. Zhang, Y. Feng, J. Zhu, J. Xu, et al., Cobalt, nitrogen-doped porous carbon nanosheet-assembled flowers from metal-coordinated covalent organic polymers for efficient oxygen reduction, ACS Appl. Mater. Interfaces 11 (2019) 1384–1393.